

Floquet Hofstadter butterfly in trilayer graphene with a twisted top layer

Nadia Benlakhrouy,^{1,*} Ahmed Jellal,^{1,2,†} and Hocine Bahlouli³

¹*Laboratory of Theoretical Physics, Faculty of Sciences,
Chouaib Doukkali University, PO Box 20, 24000 El Jadida, Morocco*

²*Canadian Quantum Research Center, 204-3002 32 Ave Vernon, BC V1T 2L7, Canada*

³*Physics Department, King Fahd University of Petroleum & Minerals, Dhahran 31261, Saudi Arabia*
(Dated: December 22, 2022)

The magnetic field generated Hofstadter butterfly in single-twist trilayer graphene (TLG) is investigated using circularly polarized light (CPL) and longitudinal light emanating from a waveguide. We show that single-twist TLG has two distinct chiral limits in the equilibrium state, and the central branch of the butterfly splits into two precisely degenerate components. The Hofstadter butterfly appears to be more discernible. We also discovered that CPL causes a large gap opening at the central branch of the Hofstadter butterfly energy spectrum and between the Landau levels, with a clear asymmetry corresponding to energy $E = 0$. We point out that for right-handed CPL, the central band shifts downward, in stark contrast to left-handed CPL, where the central band shifts upward. Finally, we investigated the effect of longitudinally polarized light, which originates from a waveguide. Interestingly, we observed that the chiral symmetries of the Hofstadter butterfly energy spectrum are broken for small driving strengths and get restored at large ones, contrary to what was observed in twisted bilayer graphene.

PACS numbers: 72.80.Vp, 73.21.-b, 71.10.Pm, 03.65.Pm

KEYWORDS: Trilayer Graphene, magic angle, magnetic field, Hofstadter butterfly, circularly polarized light, waveguide.

I. INTRODUCTION

Following the discovery of superconductivity and correlation-induced insulators, physicists have taken a keen interest in investigating further physical properties of twisted multi-layer graphene [1–4]. Most of the observed exotic phases were caused by a small twist angle between successive graphene layers, more specifically at a magic angle, where an isolated flat energy band appeared [5, 6]. Twisted bilayer graphene (TBLG) [7–24], twisted trilayer graphene (TTLG) [25–29] a variety of other multi-layer arrangements [30, 31] were among the most thoroughly studied structures, both theoretically and experimentally. The small twist between two or three layers of graphene produces a long-wavelength moiré pattern as described in Refs [7, 32–35] see Fig. 1a in particular. During the last few years, these moiré pattern systems have attracted considerable interest because they constitute a test bed for the occurrence of a variety of anomalous and highly correlated phases. The recent studies of TTLG have largely focused on the electronic structure [29], the importance of topological flat energy bands near the magic angles [36–42], and the rich optical properties [43–52]. In this context, the moiré and Floquet techniques have recently been integrated to obtain theoretical predictions regarding distinct topological phases in moiré materials [28, 35, 53–57]. Floquet’s theory has been exploited in studies concerned with the electromagnetic interaction of external light sources with materials

where light intensity and polarization have been used to control the transport properties in these devices that are based on twisted multi-layer graphene systems.

The objective of this research is to find out more about the magnetic field generated Hofstadter butterfly in single-twist TLG subjected to various types of light, including circularly polarized light (CPL) and longitudinal light emanating from a waveguide. The famous Hofstadter butterfly shows up when a two-dimensional periodic electron system is subjected to a perpendicular magnetic field, which then exhibits fractal patterns in their energy spectrum [58]. The influence of light on the Hofstadter butterfly energy spectrum has recently attracted the physics community’s curiosity [59–68]. Previous research concentrated on the kicked Harper model as well as laser-irradiated monolayer graphene (MLG) in the presence of a uniform perpendicular magnetic field B [59–63]. In our recent work in TBLG [69], we found that in the non-equilibrium situation, in the presence of light, the magnetic field generated Hofstadter butterfly exhibits a much richer structure. Recent efforts focused on investigating single-twist BLG and single-twist TLG under the effects of two kinds of light polarization, CPL and longitudinally polarized light originating from a waveguide [28, 54, 70]. CPL case was treated using a rotating frame (RF) Hamiltonian. This latter was designed to treat both strong and weak perturbations in the high to intermediate frequency ranges [70]. In addition, this Hamiltonian is valid in the ranges where the ordinary Van Vleck approximation fails. As a result, the computations of the quasi-energy levels were greatly improved. In single-twist TLG, the design of the crystalline stacking configuration, as well as the selection of which of the three layers is to be twisted, generates a distinct physical system with dif-

* benlakhrouy.n@ucd.ac.ma

† a.jellal@ucd.ac.ma

ferent characteristics [48, 49]. We focus here on the top single-layer twist with ABA stacking. We will look at the chiral case, such as TBLG, which is controlled by the interlayer coupling parameters $\omega_0 = 0$ for AA-bilayer graphene and $\omega_1 \neq 0$ for AB-bilayer graphene. It was discovered that the last hopping term plays a critical role in the creation of the flat energy bands at the magic angle [71]. The main difference here is that we find that ω_0 -type hopping is a key factor in the creation of the Hofstadter butterfly in TBLG [69]. This kept us motivated to check this feature in single-twist TLG. We start by first studying angles larger than the magic angle and intermediate twist angle, then restricting our attention to the magic angle. Furthermore, we are expecting to obtain a rich light-induced structure of the Hofstadter butterfly in single-twist TLG.

The remainder of this work is structured in the following manner. We describe single-twist TLG in Sec. II, and we base our discussion on the main features of the equilibrium state, beginning with the equilibrium model. In particular, we investigate which of the single-twist TLG's hopping processes has the greatest impact on the Hofstadter butterfly. In addition, we demonstrate how the various hopping terms affect symmetry in relation to the central branch or $E = 0$, and we investigate the impact of the twist angle on this feature. In Sec. III, a non-equilibrium case, we first discuss the effect of circularly polarised light. The second type of light polarization, longitudinal light emanating from a waveguide, is discussed in Sec. IV. Last, we summarize our main findings and present our conclusions.

II. EQUILIBRIUM STUDIES

A. Theoretical approach

To begin with, we adopt the continuum model Hamiltonian for single-twist TLG in Refs. [28, 29] with twisted top layer (TTL). The TTL can be captured by twisting the middle-bottom and top layers in opposite directions. The effective model of single-twist TLG projected onto the $+K$ valley reads as follows:

$$\mathcal{H} = \begin{pmatrix} -iv_F(\boldsymbol{\sigma}_{-\theta/2} \cdot \boldsymbol{\nabla}) & T_{12}(\mathbf{r}) & 0 \\ T_{12}^\dagger(\mathbf{r}) & -iv_F(\boldsymbol{\sigma}_{\theta/2} \cdot \boldsymbol{\nabla}) & T_{23} \\ 0 & T_{23}^\dagger & -iv_F(\boldsymbol{\sigma}_{\theta/2} \cdot \boldsymbol{\nabla}) \end{pmatrix}, \quad (1)$$

where the MLG tight-binding Hamiltonians reflecting the intralayer hopping of the l -th layer are depicted by the diagonal blocks in Eq. (1)

$$h_\ell(\theta_\ell) = -iv_F(\boldsymbol{\sigma}_{\theta_\ell} \cdot \boldsymbol{\nabla}), \quad (2)$$

where the Fermi velocity in each graphene layer is represented by $v_F = 10^6$ m/s. $\boldsymbol{\sigma} = (\sigma_x, \sigma_y)$ represent Pauli matrices acting on sublattice. TTL can be specified using parameters like $\theta_1 = -\theta/2$, and $\theta_2 = \theta_3 = \theta/2$. The rotated Pauli matrices are given by

$$\boldsymbol{\sigma}_{\theta_\ell} = (\cos(\theta_\ell)\sigma_x - \sin(\theta_\ell)\sigma_y, \cos(\theta_\ell)\sigma_x + \sin(\theta_\ell)\sigma_y). \quad (3)$$

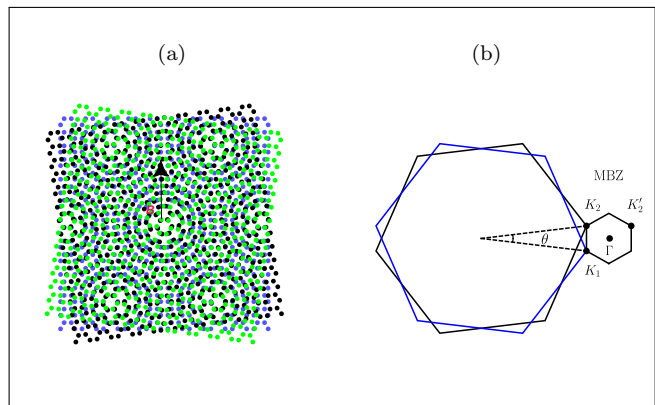


FIG. 1. (a) Illustration of the moiré pattern of twisted trilayer graphene (TTLG). (b) A schematic illustration of the moiré Brillouin zone (MBZ).

The off-diagonal block matrix elements in (1) represent interlayer hopping. They are given by

$$T_{12}(\mathbf{r}) = \sum_{j=1}^3 e^{-i\mathbf{q}_j \cdot \mathbf{r}} T_j, \quad (4)$$

$$T_{23} = \sum_{j=1}^3 T_j, \quad (5)$$

where $\mathbf{q}_1 = k_\theta(0, -1)$, $\mathbf{q}_{2,3} = k_\theta(\pm\sqrt{3}, 1)$ are the MBZ's nearest neighbor vectors with the modulation $k_\theta = 2k_D \sin(\frac{\theta}{2})$. The Dirac momentum is represented by $k_D = 4\pi/3a_0$, with $a_0 = 2.46$ Å the lattice constant. In the case of TTL, T_{23} is position independent [28, 29]. The matrices T_j take into account tunneling between sublattice and depend on the type of stacking. [29]. They have the following structure

$$T_j^{\text{AB}} = [T_j^{\text{BA}}]^\dagger = \begin{pmatrix} \omega_0 e^{i\frac{2j\pi}{3}} & \omega_1 \\ \omega_1 e^{-i\frac{2j\pi}{3}} & \omega_0 e^{i\frac{2j\pi}{3}} \end{pmatrix}, \quad (6)$$

$$T_j^{\text{AA}} = \begin{pmatrix} \omega_0 & \omega_1 e^{-i\frac{2j\pi}{3}} \\ \omega_1 e^{i\frac{2j\pi}{3}} & \omega_0 \end{pmatrix}. \quad (7)$$

Because AB and BA stacking are more energetically favorable than AA stacked regions [54, 72, 73], we added a parameter ω_i to the tunneling term to represent the effect of relaxation. Additionally, AA and AB regions offer distinct interlayer-lattice constants [74]. In our case, we take these variables into account in the hopping amplitudes by considering $(\omega_0, \omega_1) = (80 \text{ meV}/80 \text{ meV}, 110 \text{ meV})$ for (AB/BA, AA)-type hopping amplitude. In a relaxed lattice, distortions can be detected in this way [28, 54, 73] if the next neighboring layer interactions are neglected, making them comparable to those in TBLG.

B. Interlayer hopping and the Hofstadter butterfly

The energy spectrum was calculated numerically using the assumption that [5]

$$N_{\text{max}} \approx 2 \left[\frac{\max(a_0 \gamma_{\text{RF}}, \omega_1)}{\omega_c} \right]^2. \quad (8)$$

The center of our plot, which corresponds to $E = 0$, or more precisely, $n_{LL} = 0$, splits into two precisely degenerate components and shifts to higher and lower energies $69.075 \text{ meV} \lesssim E[\text{meV}] \lesssim -62.3541 \text{ meV}$ at an intermediate twist angle of $\theta = 2^\circ$. Moreover, for small enough magnetic fields, mini gaps as wide as 332.141 meV started to appear between LLs. According to T_{12} , Eq. A11 (see App. A), every single Landau level (LL) is divided into q sub-bands and linked together. To better understand the Hofstadter butterfly in TTLG ABA TTL devices, we propose a second twist angle, which we prefer to call the magic angle $\theta_M = 1.6^\circ$ with $\omega_0/\omega_1 \simeq 0.8$. Here the Hofstadter butterfly structure appears, see Fig. 2b, and the band gaps are minimized for the small magic angles. Previous studies on the square, honeycomb, and kagome lattices [75] and TBLG [69] investigated a rich symmetry with $\alpha = 0.5$ and a reflection symmetry with $E = 0$. In contrast to the single-twist TLG, we notice that the reflection symmetry concerning the axis of energy $E = 0$ is somewhere missing due to the interlayer hopping terms.

The next step in our equilibrium investigation will be to determine whether ω_0 or ω_1 interlayer hopping processes are more important than the other for the appearance of our butterfly in single-twist TLG, as done in TBLG studies [69]. In Fig. 2c, we show the Hofstadter butterfly in the chiral model [71], which is equivalent to $\omega_0 = 0$. As expected, our plot's center merges into a zero-energy line. This is because graphene has a single sublattice with the lowest LL, and the parameters in $T(\mathbf{r})$ that connect sublattices are directly proportional to w_1 . Consequently, the lowest LL is unaffected by these terms. In comparison to higher levels, this is a significant difference, which persists in both sublattices. As previously stated, we take $V = T(\mathbf{r})$ as a result of perturbation, then the lowest LLs eigen-bi-spinors for $T(\mathbf{r}) = 0$ satisfy $|L_{01}\rangle = (0, |0\rangle, 0, 0)$ or $|L_{02}\rangle = (0, 0, 0, |0\rangle)$. The first energy correction as a consequence of this can be expressed as $\langle L_{02}|V|L_{02}\rangle = 0$ for $w_0 = 0$. As a result, the lowest LL remains unsplit. It's worth noting that the other LLS also start to collapse on each other more than in the case of TBLG [69]. For example, we can observe that ω_0 influences the strength of the lowest LL splitting. The ω_0 -type hoppings then become less important in single-twist TLG [76] for small magic angles. Now consider the opposite situation, $\omega_1 = 0$ and $\omega_0 = 110 \text{ meV}$, as shown in Fig. 2d. Remarkably, we recognize that in these circumstances, it is this term that leads the center LL

to split and the Hofstadter butterfly to appear. Tarnopolsky and colleagues [71] investigated the lower relevant term that allows the flat band to appear.

III. CIRCULARLY POLARIZED LIGHT

In this part, we will look at how the circularly polarized light (CPL) affects the Hofstadter butterfly in single-twist TLG.

A. Effective Hamiltonian

We assume CPL is transmitted perpendicular to the single-twist TLG at frequency Ω and driving strength A . Eventually, light comes into play through the usual minimal substitution [28, 70, 77]

$$k_x \rightarrow k_x(t) = k_x - A \cos(\Omega t), \quad (9)$$

$$k_y \rightarrow \tilde{k}_y = k_y - A \sin(\Omega t). \quad (10)$$

As a result, we obtain a time-periodic Hamiltonian $H(\mathbf{x}, \mathbf{k}, t) = H(\mathbf{x}, \mathbf{k}, t + 2\pi/\Omega)$. It is well known that such a Hamiltonian can be accurately replaced by an effective time-independent Hamiltonian [70]. A numerically advantageous and less costly approach would be helpful in the current situation. Therefore, let us quickly examine how to derive an effective time-dependent description and what new physical phenomena can emerge from it. Converting a regularly driven Hamiltonian into an RF is a non-perturbative way of finding the effective time-independent Hamiltonian. The following transformation can be used for this purpose [70]:

$$H_R = U^\dagger(t) (H - i\partial_t) U(t). \quad (11)$$

A Hamiltonian is generated by a subsequent time average if a suitable frame is selected. This is a more honest description than Hamiltonians generated by van Vleck or Floquet-Magnus approximations, which are common high frequency regimes [78]. It was revealed that using a well-chosen unitary transformation [28, 70] that for single-twist TLG subjected to CPL, a highly accurate effective Hamiltonian will result

$$\mathcal{H}(\mathbf{r}, t) = \begin{pmatrix} v_{\text{RF}} R(\theta_1) \mathbf{k} \cdot \boldsymbol{\sigma} - \Delta_{\text{RF}} \sigma_3 & \tilde{T}_{12}(\mathbf{r}) & 0 \\ \tilde{T}_{12}^\dagger(\mathbf{r}) & v_{\text{RF}} R(\theta_2) \mathbf{k} \cdot \boldsymbol{\sigma} - \Delta_{\text{RF}} \sigma_3 & \tilde{T}_{23} \\ 0 & \tilde{T}_{23}^\dagger & v_{\text{RF}} R(\theta_3) \mathbf{k} \cdot \boldsymbol{\sigma} - \Delta_{\text{RF}} \sigma_3 \end{pmatrix}, \quad (12)$$

where $R(\theta)$ denotes the rotation matrix. The Fermi velocity has been affected and is now equal to

$$v_{\text{RF}} = v_F J_0 \left(-\frac{6\gamma}{\Omega} J_1 \left(\frac{2Aa_0}{3} \right) \right) J_0 \left(\frac{2Aa_0}{3} \right), \quad (13)$$

J_0 is the zeroth Bessel function of the first kind. Light also provokes the system to create a band gap, which is expressed as

$$\Delta_{\text{RF}} = -\frac{3\gamma}{\sqrt{2}} J_1 \left(\frac{2Aa_0}{3} \right) J_1 \left(-\frac{6\sqrt{2}\gamma}{\Omega} J_1 \left(\frac{2Aa_0}{3} \right) \right). \quad (14)$$

Interlayer tunneling matrices Eq. 6 are also modified. Now if we express T_j as $T_j = \sum_i T_{j,i} \sigma_i$, where $T_{j,n}$ are expansion coefficients, we get the new hopping matrices \tilde{T}_j

$$\tilde{T}_j^{\text{AB}} = [\tilde{T}_j^{\text{BA}}]^\dagger = \sum_i T_{j,i} \tilde{\sigma}_i, \quad (15)$$

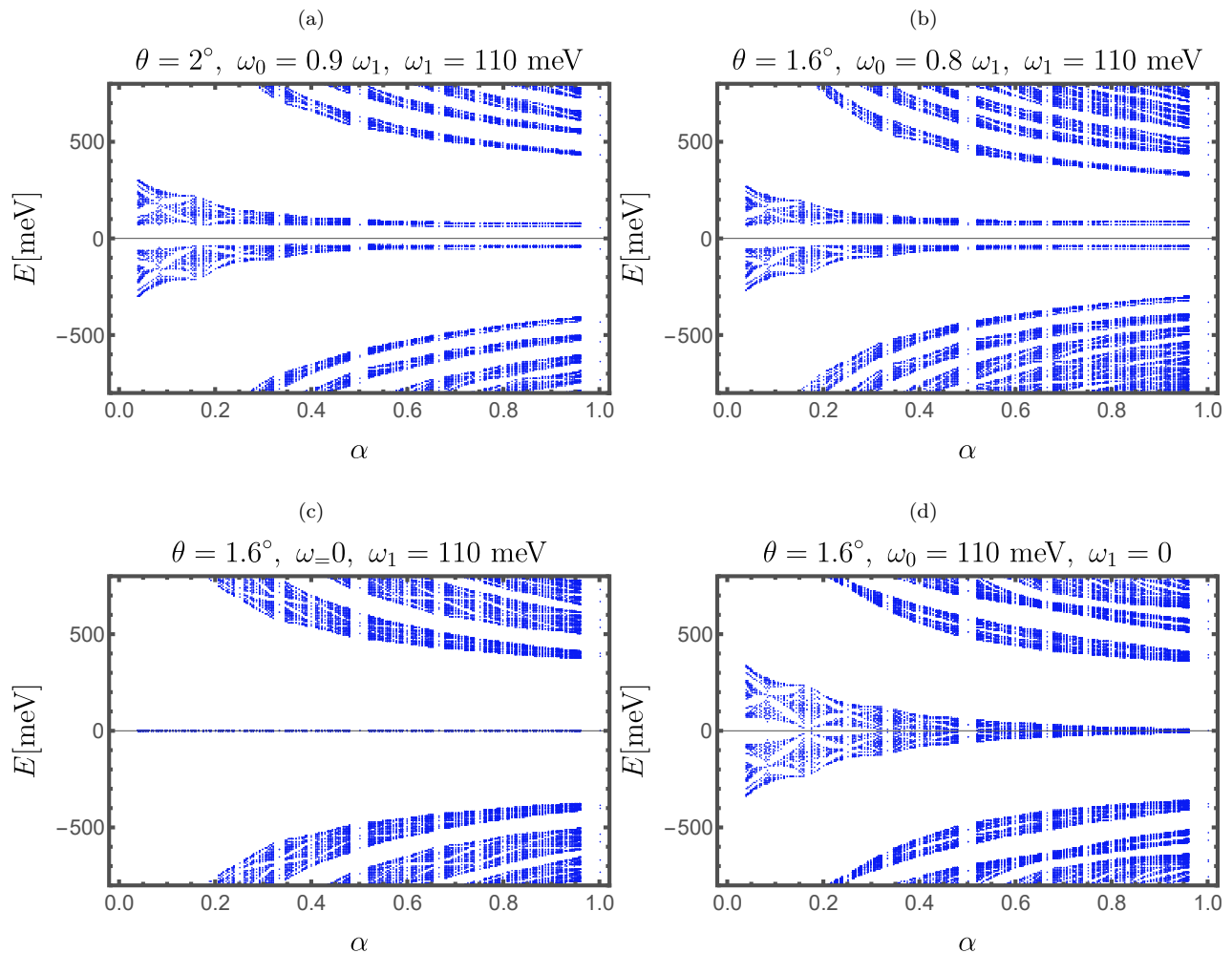


FIG. 2. (Color online) The numerically generated Hofstadter butterfly spectrum for single-twist TLG with parameters (a) $(\theta, \omega_0, \omega_1) = (2^\circ, 0.9\omega_1, 110 \text{ meV})$, (b) $(\theta, \omega_0, \omega_1) = (1.6^\circ, 0.8\omega_1, 110 \text{ meV})$, (c) $(\theta, \omega_0, \omega_1) = (1.6^\circ, 0, 110 \text{ meV})$, (d) $(\theta, \omega_0, \omega_1) = (1.6^\circ, 110 \text{ meV}, 0)$.

with the matrices

$$\tilde{\sigma}_{1,2} = J_0(\nu)\sigma_{1,2}, \quad (16)$$

$$\tilde{\sigma}_{0,3} = \sigma_{0,3} + \left(J_0(\sqrt{2}\nu) - 1 \right) \left[\sigma_{0,3} \sin^2 \left(\frac{\theta}{2} \right) \pm \frac{i}{2} \sigma_3 \sin(\theta) \right]. \quad (17)$$

where $\nu = (-6\gamma/\Omega)J_1(2Aa_0/3)$, and $\sigma_{1,2,3}$ are the Pauli matrices, and σ_0 is the identity matrix.

B. Numerical Results

In this section, we look at how CPL influences the Hofstadter butterfly in single-twist TLG. To achieve this, in Fig. 3, we plotted the Hofstadter butterfly resulting from this form of light. For certain twist angles ($\theta = 1.6^\circ/\theta = 1.8^\circ$), driving strength $Aa_0 = 0.15$, $Aa_0 = 0.25$, $Aa_0 = 0.3$, and driving frequency $\Omega = 2\gamma$, and $\Omega = 3\gamma$, CPL has an interesting effects. Indeed, the associated energy levels split as we increase the driving strength and the driving frequency. The

0-th LLs of the butterfly's central branch move upwards to higher energies and are separated as shown in Fig. 3a. As a result, the spectrum appears to be asymmetrical with respect to $E = 0$ because the band-gap Δ_{RF} violates chiral symmetry. Compared to TBLG [69] we note that the gaps between LLs increase in single-twist TLG. As a result, it's an appealing choice in strongly correlated phases, since interactions are expected to dominate in this case, as discussed in [28]. We highlight that the central LL is shifted upward in Figs. Figs. 3a, 3b, 3c, and 3d since we are considering right-handed CPL. Additionally, switching from a right-handed to a left-handed CPL results in the substitution

$$\Delta_{\text{RF}} \mapsto -\Delta_{\text{RF}}. \quad (18)$$

We plot the Hofstadter butterfly subject to left-handed CPL in Fig. 3a and 3b with the same values as in Fig. 3a and 3b. We observe that the central Landau level has been pushed downward.

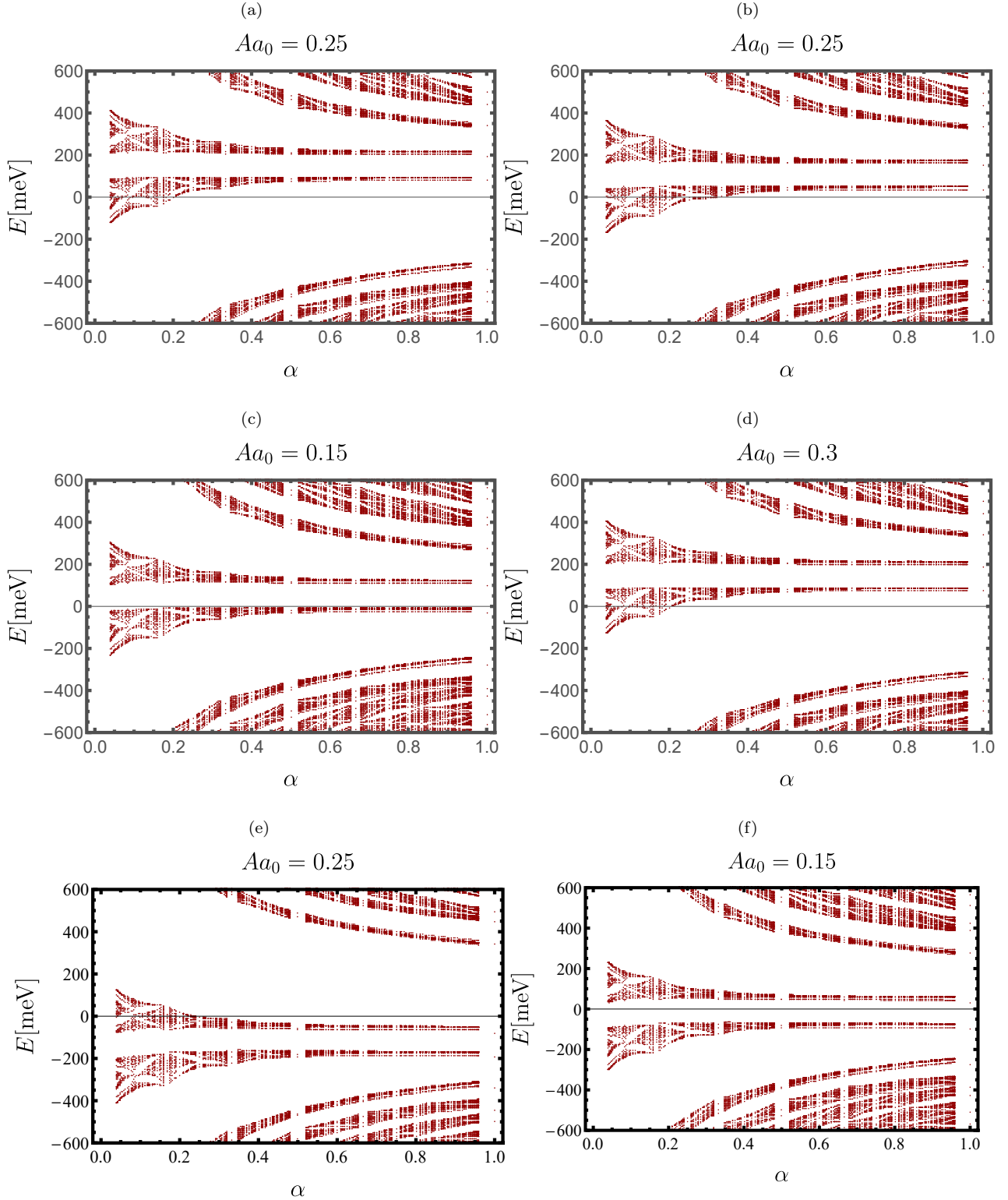


FIG. 3. (Color online) The numerically generated Floquet Hofstadter butterfly spectrum subjected to a right-handed CPL with parameters: $\omega_0 = 0.8$, $\omega_1 = 110$ meV, (a) $(\theta, Aa_0, \Omega) = (1.8^\circ, 0.25, 2\gamma)$, (b) $(\theta, Aa_0, \Omega) = (1.8^\circ, 0.25, 3\gamma)$, (c) $(\theta, Aa_0, \Omega) = (1.6^\circ, 0.15, 3\gamma)$, and (d) $(\theta, Aa_0, \Omega) = (1.8^\circ, 0.3, 3\gamma)$. Energy spectrum of the Floquet Hofstadter butterfly subjected to left-handed CPL with the parameters: (e) $(\theta, Aa_0, \Omega) = (1.8^\circ, 0.25, 2\gamma)$, and (f) $(\theta, Aa_0, \Omega) = (1.6^\circ, 0.15, 3\gamma)$.

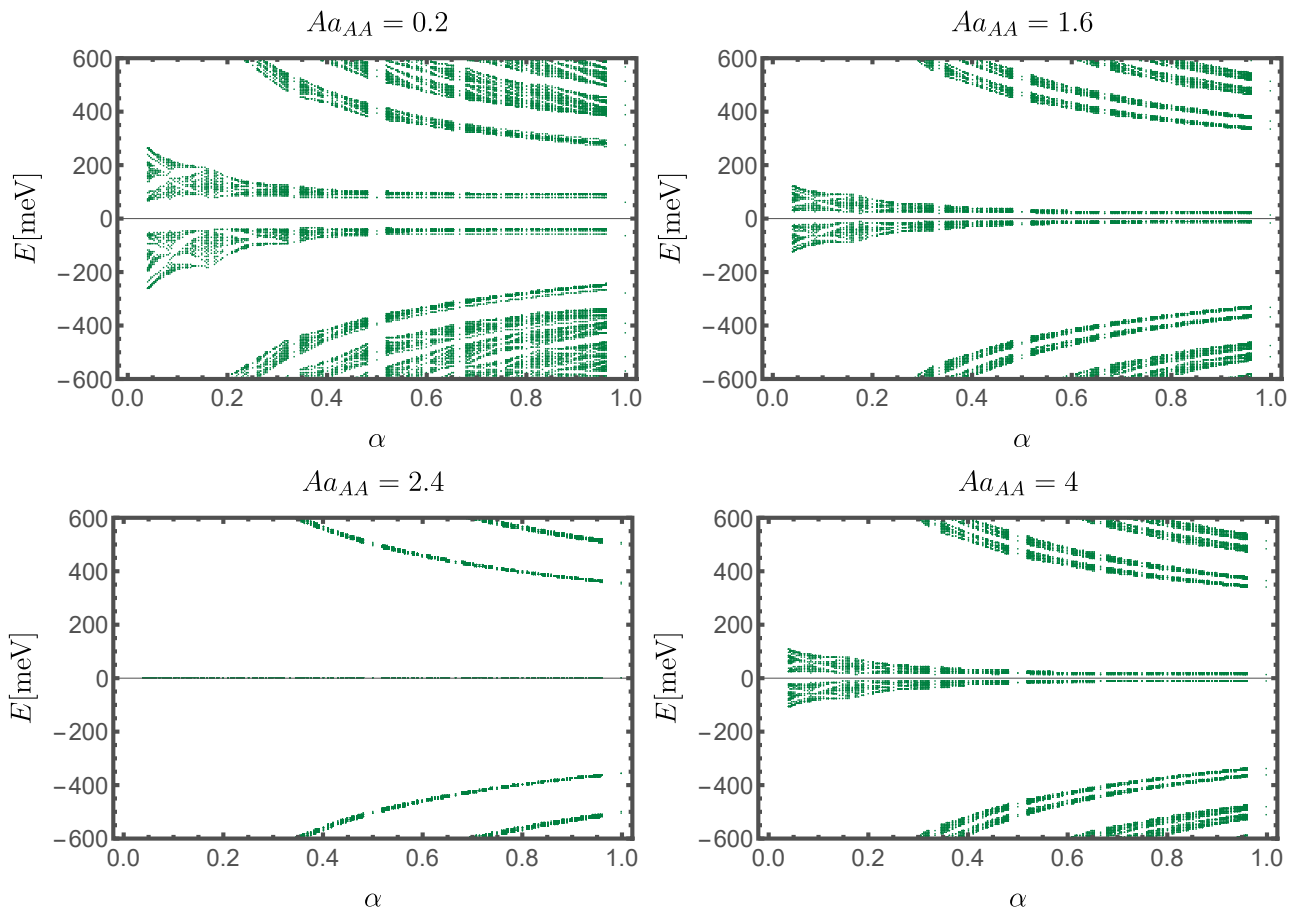


FIG. 4. (Color online) The numerically generated Floquet Hofstadter butterfly spectrum subjected to a waveguide light. The following driving strengths have been used $Aa_{AA} = 0.2$ to $Aa_{AA} = 4$ in addition to the parameters $\gamma = 2364$ meV, and $\theta = 1.6^\circ$.

IV. WAVEGUIDE LIGHT

Following our study of CPL in the previous section, we will look at the impact of longitudinal light originating from a waveguide on our TTLG spectrum.

A. Theoretical Approach

We will now consider longitudinal light emanating from a waveguide, as a second type of light. In this situation, the waveguide's boundary conditions allow light to have longitudinal components $\mathbf{A} = \text{Re}(e^{ik_z z - i\Omega t}) \hat{z}$ to occur in a vacuum (More details on the derivation can be found in [54] or the most popular references on electromagnetism [79]). The effect of this type of light can be investigated at the tight-binding level through a Peirls substitution

$$t_{ij} \rightarrow t_{ij} e^{(-\int_{r_i}^{r_j} \mathbf{A} \cdot d\mathbf{l})}, \quad (19)$$

where \mathbf{A} is the vector potential. In the continuum, Hamiltonian hopping terms refer to ω_i , which is now

$$w_i \rightarrow w_i e^{(-\int_{r_i}^{r_j} \mathbf{A} \cdot d\mathbf{l})}. \quad (20)$$

This phenomenon can be incorporated in the high frequency domain of our continuum model by modifying interlayer couplings as shown below

$$\begin{aligned} \omega_1 &\rightarrow \tilde{\omega}_1 = J_0(|Aa_{AB}|)\omega_1, \\ \omega_0 &\rightarrow \tilde{\omega}_0 = J_0(|Aa_{AA}|)\omega_0, \end{aligned} \quad (21)$$

where $a_{AA} = 0.36$ nm and $a_{AB} = 0.34$ nm are interlayer distances in the regions AA, and AB respectively.

B. Numerical Results

Next, we will start examining how the waveguide light affects the Hofstadter butterfly in single-twist TLG using our numerical results. Similarly to TBLG [69], we consider a range of distinct values Aa_{AA} for our unit-less driving strength. It should be remembered that

$$\frac{Aa_{AB}}{Aa_{AA}} = \frac{a_{AB}}{a_{AA}}. \quad (22)$$

Fig. 4 considers various values ranging from $Aa_{AA} = 0.2$ to 4. We notice that as Aa_{AA} increases, the individual LL splitting decreases at first, and then increases. To better understand these splittings, we plot the renormalized hopping

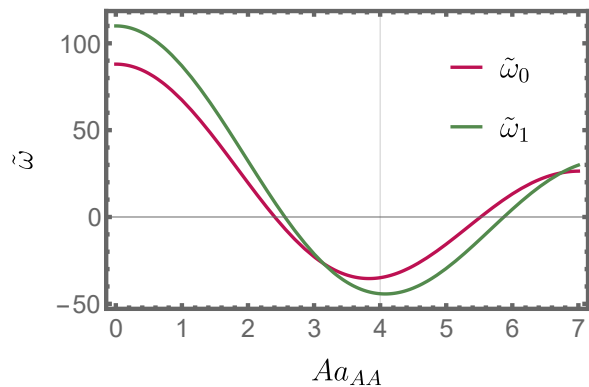


FIG. 5. (Color online) Plot of the renormalized hopping amplitude $\tilde{\omega}_0$ and $\tilde{\omega}_1$ as function of the deriving strength Aa_{AA} .

amplitudes $\tilde{\omega}_0$ and $\tilde{\omega}_1$ as a function of the deriving strength Aa_{AA} in Fig. 5. As shown, the hopping amplitudes $\tilde{\omega}_0$ and $\tilde{\omega}_1$ initially decrease to be minimal for small values of the derived strength Aa_{AA} . Both quantities increase after $Aa_{AA} = 4$, but $\tilde{\omega}_0$ becomes more important than $\tilde{\omega}_1$. In our case, this is modulated by the Bessel function J_0 , which determines the magnitude of level splitting. We conclude that Bessel functions influence the interlayer hoppings in single-twist TLG as it was also noticed in [69]. Of course, this finding allows us to go one step further and conclude that the two chiral models $\omega_1 = 0$ or $\omega_0 = 0$ can both be generated using this type of light. Particularly, if $Aa_{AA} = j_{0,n}$ is the n -th zero Bessel function $J_0(x)$, ω_0 is completely set to 0. Moreover, ω_1 is 0 unless $Aa_{AA} = (a_{AA}/a_{AB})j_{0,n}$. We notice that the gap opening in this situation starts to close at $AaA = 1.6$. Under these circumstances, and in contrast to the case of CPL, with respect to $E = 0$, mirror symmetry of our energy spectrum remains intact.

V. CONCLUSION

The current study investigated the magnetic field induced Floquet Hofstadter butterfly spectrum in a top twisted ABA stacked trilayer graphene in the presence of a perpendicular magnetic field. We first investigated the characteristics of the equilibrium state of the system in the absence of light, and after that, we went on to study different non-equilibrium situations. We specifically considered the presence of circularly polarized light and waveguide linearly polarized light. In the equilibrium state, the butterfly's central branch splits into two precisely degenerate components, and for small twist angles, such as $\theta_M = 1.6^\circ$, our butterfly becomes more discernible.

Afterward, we have identified that the effect of interlayer coupling ω_0 in the AA stacking type hopping terms is much more important than the interlayer ω_1 in the AB/BA stacking type on the appearance of the Hofstadter butterfly. We also came to the conclusion that single-twist TLG has two separate chiral limits, similarly to TBLG. In the non-equilibrium case, in the presence of a CPL, we showed how this type of light causes large gap openings at the central branch of the Hofstadter butterfly with clearly discernible asymmetry with regard to energy $E = 0$. In addition, for right-handed CPL, the central band shifts downward, in stark contrast to left-handed CPL, where the central band shifts upward. We also investigated the effect of longitudinally polarized light emanating from a waveguide on the Hofstadter butterfly spectrum in single-twist TLG. We showed that in the case of waveguide light, chiral symmetries are broken at small driving strengths and restored at large driving strengths, contrary to previous observations in TBLG.

Acknowledgment: The authors deeply appreciate discussions with Michael Vogl on the subject matter of this paper.

-
- [1] Allan H MacDonald. Bilayer graphene's wicked, twisted road. *Physics*, 12:12, 2019.
 - [2] Eva Y Andrei and Allan H MacDonald. Graphene bilayers with a twist. *Nature materials*, 19(12):1265–1275, 2020.
 - [3] Dante M Kennes, Martin Claassen, Lede Xian, Antoine Georges, Andrew J Millis, James Hone, Cory R Dean, DN Basov, Abhay N Pasupathy, and Angel Rubio. Moiré heterostructures as a condensed-matter quantum simulator. *Nature Physics*, 17(2):155–163, 2021.
 - [4] Leon Balents, Cory R Dean, Dmitri K Efetov, and Andrea F Young. Superconductivity and strong correlations in moiré flat bands. *Nature Physics*, 16(7):725–733, 2020.
 - [5] Rafi Bistritzer and Allan H MacDonald. Moiré bands in twisted double-layer graphene. *Proceedings of the National Academy of Sciences*, 108(30):12233–12237, 2011.
 - [6] JMB Lopes Dos Santos, NMR Peres, and AH Castro Neto. Continuum model of the twisted graphene bilayer. *Physical Review B*, 86(15):155449, 2012.
 - [7] Yuan Cao, Valla Fatemi, Shiang Fang, Kenji Watanabe, Takashi Taniguchi, Efthimios Kaxiras, and Pablo Jarillo-Herrero. Unconventional superconductivity in magic-angle graphene superlattices. *Nature*, 556(7699):43–50, 2018.
 - [8] Yuan Cao, Daniel Rodan-Legrain, Oriol Rubies-Bigorda, Jeong Min Park, Kenji Watanabe, Takashi Taniguchi, and Pablo Jarillo-Herrero. Tunable correlated states and spin-polarized phases in twisted bilayer–bilayer graphene. *Nature*, 583(7815):215–220, 2020.
 - [9] Leonardo A Navarro-Labastida, Abdiel Espinosa-Champo, Enrique Aguilar-Mendez, and Gerardo G Naumis. Why the first magic-angle is different from others in twisted graphene bilayers: Interlayer currents, kinetic and confinement energy, and wave-function localization. *Physical Review B*, 105(11):115434, 2022.
 - [10] Gerardo G Naumis, Leonardo A Navarro-Labastida, Enrique Aguilar-Méndez, and Abdiel Espinosa-Champo. Reduction of the twisted bilayer graphene chiral hamiltonian into a 2×2 matrix operator and physical origin of flat bands at magic angles. *Physical Review B*, 103(24):245418, 2021.
 - [11] Cheng Shen, Yanbang Chu, QuanSheng Wu, Na Li, Shuopei Wang, Yanchong Zhao, Jian Tang, Jiaying Liu, Jinpeng Tian, Kenji Watanabe, et al. Correlated states

- in twisted double bilayer graphene. *Nature Physics*, 16(5):520–525, 2020.
- [12] Xiaomeng Liu, Zeyu Hao, Eslam Khalaf, Jong Yeon Lee, Yuval Ronen, Hyobin Yoo, Danial Haei Najafabadi, Kenji Watanabe, Takashi Taniguchi, Ashvin Vishwanath, et al. Tunable spin-polarized correlated states in twisted double bilayer graphene. *Nature*, 583(7815):221–225, 2020.
- [13] Narasimha Raju Chebrolu, Bheema Lingam Chittari, and Jeil Jung. Flat bands in twisted double bilayer graphene. *Physical Review B*, 99(23):235417, 2019.
- [14] Mikito Koshino. Band structure and topological properties of twisted double bilayer graphene. *Physical Review B*, 99(23):235406, 2019.
- [15] Jong Yeon Lee, Eslam Khalaf, Shang Liu, Xiaomeng Liu, Zeyu Hao, Philip Kim, and Ashvin Vishwanath. Theory of correlated insulating behaviour and spin-triplet superconductivity in twisted double bilayer graphene. *Nature communications*, 10(1):1–10, 2019.
- [16] Fatemeh Haddadi, QuanSheng Wu, Alex J Kruchkov, and Oleg V Yazyev. Moiré flat bands in twisted double bilayer graphene. *Nano letters*, 20(4):2410–2415, 2020.
- [17] Francisco Javier Culchac, RR Del Grande, Rodrigo B Capaz, Leonor Chico, and E Suárez Morell. Flat bands and gaps in twisted double bilayer graphene. *Nanoscale*, 12(8):5014–5020, 2020.
- [18] Ya-Hui Zhang, Dan Mao, Yuan Cao, Pablo Jarillo-Herrero, and T Senthil. Nearly flat chern bands in moiré superlattices. *Physical Review B*, 99(7):075127, 2019.
- [19] Dillon Wong, Kevin P Nuckolls, Myungchul Oh, Biao Lian, Yonglong Xie, Sangjun Jeon, Kenji Watanabe, Takashi Taniguchi, B Andrei Bernevig, and Ali Yazdani. Cascade of electronic transitions in magic-angle twisted bilayer graphene. *Nature*, 582(7811):198–202, 2020.
- [20] Xiaobo Lu, Petr Stepanov, Wei Yang, Ming Xie, Mohammed Ali Aamir, Ipsita Das, Carles Urgell, Kenji Watanabe, Takashi Taniguchi, Guangyu Zhang, et al. Superconductors, orbital magnets and correlated states in magic-angle bilayer graphene. *Nature*, 574(7780):653–657, 2019.
- [21] Ipsita Das, Cheng Shen, Alexandre Jaoui, Jonah Herzog-Arbeitman, Aaron Chew, Chang-Woo Cho, Kenji Watanabe, Takashi Taniguchi, Benjamin A. Piot, B. Andrei Bernevig, and Dmitri K. Efetov. Observation of reentrant correlated insulators and interaction-driven fermi-surface reconstructions at one magnetic flux quantum per moiré unit cell in magic-angle twisted bilayer graphene. *Phys. Rev. Lett.*, 128:217701, 2022.
- [22] Jonah Herzog-Arbeitman, Aaron Chew, Dmitri K. Efetov, and B. Andrei Bernevig. Reentrant correlated insulators in twisted bilayer graphene at 25 t (2π flux). *Phys. Rev. Lett.*, 129:076401, 2022.
- [23] Jonah Herzog-Arbeitman, Aaron Chew, and B Andrei Bernevig. Magnetic bloch theorem and reentrant flat bands in twisted bilayer graphene at 2π flux. *Physical Review B*, 106(8):085140, 2022.
- [24] Jiachen Yu, Benjamin A Foutty, Zhaoyu Han, Mark E Barber, Yoni Schattner, Kenji Watanabe, Takashi Taniguchi, Philip Phillips, Zhi-Xun Shen, Steven A Kivelson, et al. Correlated hofstadter spectrum and flavour phase diagram in magic-angle twisted bilayer graphene. *Nature Physics*, pages 1–7, 2022.
- [25] Jeong Min Park, Yuan Cao, Kenji Watanabe, Takashi Taniguchi, and Pablo Jarillo-Herrero. Tunable strongly coupled superconductivity in magic-angle twisted trilayer graphene. *Nature*, 590(7845):249–255, 2021.
- [26] Zeyu Hao, AM Zimmerman, Patrick Ledwith, Eslam Khalaf, Danial Haie Najafabadi, Kenji Watanabe, Takashi Taniguchi, Ashvin Vishwanath, and Philip Kim. Electric field-tunable superconductivity in alternating-twist magic-angle trilayer graphene. *Science*, 371(6534):1133–1138, 2021.
- [27] Alejandro Lopez-Bezanilla and JL Lado. Electrical band flattening, valley flux, and superconductivity in twisted trilayer graphene. *Physical Review Research*, 2(3):033357, 2020.
- [28] IA Assi, JPF LeBlanc, Martin Rodriguez-Vega, Hocine Bahlouli, and Michael Vogl. Floquet engineering and nonequilibrium topological maps in twisted trilayer graphene. *Physical Review B*, 104(19):195429, 2021.
- [29] Xiao Li, Fengcheng Wu, and Allan H MacDonald. Electronic structure of single-twist trilayer graphene. *arXiv preprint arXiv:1907.12338*, 2019.
- [30] Alexander Kerelsky, Carmen Rubio-Verdú, Lede Xian, Dante M Kennes, Dorri Halbertal, Nathan Finney, Larry Song, Simon Turkel, Lei Wang, Kenji Watanabe, et al. Moiréless correlations in abca graphene. *Proceedings of the National Academy of Sciences*, 118(4), 2021.
- [31] Carmen Rubio-Verdú, Simon Turkel, Larry Song, Lennart Klebl, Rhine Samajdar, Mathias S Scheurer, Jörn WF Venderbos, Kenji Watanabe, Takashi Taniguchi, Héctor Ochoa, et al. Universal moiré nematic phase in twisted graphitic systems. *arXiv preprint arXiv:2009.11645*, 2020.
- [32] Kaihui Liu, Liming Zhang, Ting Cao, Chenhao Jin, Diana Qiu, Qin Zhou, Alex Zettl, Peidong Yang, Steve G Louie, and Feng Wang. Evolution of interlayer coupling in twisted molybdenum disulfide bilayers. *Nature communications*, 5(1):1–6, 2014.
- [33] Y Cao, JY Luo, V Fatemi, S Fang, JD Sanchez-Yamagishi, K Watanabe, T Taniguchi, E Kaxiras, and Pablo Jarillo-Herrero. Superlattice-induced insulating states and valley-protected orbits in twisted bilayer graphene. *Physical review letters*, 117(11):116804, 2016.
- [34] Kyoungwan Kim, Ashley DaSilva, Shengqiang Huang, Babak Fallahazad, Stefano Larentis, Takashi Taniguchi, Kenji Watanabe, Brian J LeRoy, Allan H MacDonald, and Emanuel Tutuc. Tunable moiré bands and strong correlations in small-twist-angle bilayer graphene. *Proceedings of the National Academy of Sciences*, 114(13):3364–3369, 2017.
- [35] Guohong Li, A Luican, JMB Lopes dos Santos, AH Castro Neto, A Reina, J Kong, and EY Andrei. Observation of van hove singularities in twisted graphene layers. *Nature physics*, 6(2):109–113, 2010.
- [36] Hoi Chun Po, Liujun Zou, Ashvin Vishwanath, and T Senthil. Origin of mott insulating behavior and superconductivity in twisted bilayer graphene. *Physical Review X*, 8(3):031089, 2018.
- [37] Liujun Zou, Hoi Chun Po, Ashvin Vishwanath, and T Senthil. Band structure of twisted bilayer graphene: Emergent symmetries, commensurate approximants, and wannier obstructions. *Physical Review B*, 98(8):085435, 2018.
- [38] Noah FQ Yuan and Liang Fu. Model for the metal-insulator transition in graphene superlattices and beyond. *Physical Review B*, 98(4):045103, 2018.
- [39] Jian Kang and Oskar Vafeek. Symmetry, maximally localized wannier states, and a low-energy model for twisted

- bilayer graphene narrow bands. *Physical Review X*, 8(3):031088, 2018.
- [40] Mikito Koshino, Noah FQ Yuan, Takashi Koretsune, Masayuki Ochi, Kazuhiko Kuroki, and Liang Fu. Maximally localized wannier orbitals and the extended hubbard model for twisted bilayer graphene. *Physical Review X*, 8(3):031087, 2018.
- [41] Kasra Hejazi, Chunxiao Liu, Hassan Shapourian, Xiao Chen, and Leon Balents. Multiple topological transitions in twisted bilayer graphene near the first magic angle. *Physical Review B*, 99(3):035111, 2019.
- [42] Hoi Chun Po, Liujuan Zou, T Senthil, and Ashvin Vishwanath. Faithful tight-binding models and fragile topology of magic-angle bilayer graphene. *Physical Review B*, 99(19):195455, 2019.
- [43] Wei-Jie Zuo, Jia-Bin Qiao, Dong-Lin Ma, Long-Jing Yin, Gan Sun, Jun-Yang Zhang, Li-Yang Guan, and Lin He. Scanning tunneling microscopy and spectroscopy of twisted trilayer graphene. *Physical Review B*, 97(3):035440, 2018.
- [44] Julian D Correa, Monica Pacheco, and Eric Suárez Morell. Optical absorption spectrum of rotated trilayer graphene. *Journal of Materials Science*, 49(2):642–647, 2014.
- [45] E Suárez Morell, M Pacheco, Leonor Chico, and Luis Brey. Electronic properties of twisted trilayer graphene. *Physical Review B*, 87(12):125414, 2013.
- [46] Jia-Bin Qiao and Lin He. In-plane chiral tunneling and out-of-plane valley-polarized quantum tunneling in twisted graphene trilayer. *Physical Review B*, 90(7):075410, 2014.
- [47] Christophe Mora, Nicolas Regnault, and B Andrei Bernevig. Flatbands and perfect metal in trilayer moiré graphene. *Physical review letters*, 123(2):026402, 2019.
- [48] Masato Aoki and Hiroshi Amawashi. Dependence of band structures on stacking and field in layered graphene. *Solid State Communications*, 142(3):123–127, 2007.
- [49] Changhua Bao, Wei Yao, Eryin Wang, Chaoyu Chen, José Avila, Maria C Asensio, and Shuyun Zhou. Stacking-dependent electronic structure of trilayer graphene resolved by nanoscale angle-resolved photoemission spectroscopy. *Nano letters*, 17(3):1564–1568, 2017.
- [50] AB Kuzmenko, Iris Crassee, Dirk Van Der Marel, P Blake, and KS Novoselov. Determination of the gate-tunable band gap and tight-binding parameters in bilayer graphene using infrared spectroscopy. *Physical Review B*, 80(16):165406, 2009.
- [51] Fengcheng Wu, Allan H MacDonald, and Ivar Martin. Theory of phonon-mediated superconductivity in twisted bilayer graphene. *Physical review letters*, 121(25):257001, 2018.
- [52] Bart Partoens and FM Peeters. From graphene to graphite: Electronic structure around the k point. *Physical Review B*, 74(7):075404, 2006.
- [53] Gabriel E Topp, Gregor Jotzu, James W McIver, Lede Xian, Angel Rubio, and Michael A Sentef. Topological floquet engineering of twisted bilayer graphene. *Physical Review Research*, 1(2):023031, 2019.
- [54] Michael Vogl, Martin Rodriguez-Vega, and Gregory A Fiete. Floquet engineering of interlayer couplings: Tuning the magic angle of twisted bilayer graphene at the exit of a waveguide. *Physical Review B*, 101(24):241408, 2020.
- [55] Ming Lu, Jiang Zeng, Haiwen Liu, Jin-Hua Gao, and XC Xie. Valley-selective floquet chern flat bands in twisted multilayer graphene. *Physical Review B*, 103(19):195146, 2021.
- [56] Martin Rodriguez-Vega, Michael Vogl, and Gregory A Fiete. Floquet engineering of twisted double bilayer graphene. *Physical Review Research*, 2(3):033494, 2020.
- [57] Kasra Hejazi, Chunxiao Liu, and Leon Balents. Landau levels in twisted bilayer graphene and semiclassical orbits. *Physical Review B*, 100(3):035115, 2019.
- [58] Douglas R Hofstadter. Energy levels and wave functions of bloch electrons in rational and irrational magnetic fields. *Physical review B*, 14(6):2239, 1976.
- [59] Wen-Xiao Wang, Long-Jing Yin, Jia-Bin Qiao, Tuocheng Cai, Si-Yu Li, Rui-Fen Dou, Jia-Cai Nie, Xiaosong Wu, and Lin He. Atomic resolution imaging of the two-component dirac-landau levels in a gapped graphene monolayer. *Physical Review B*, 92(16):165420, 2015.
- [60] Jiao Wang, Anders S Mouritzen, and Jiangbin Gong. Quantum control of ultra-cold atoms: uncovering a novel connection between two paradigms of quantum nonlinear dynamics. *Journal of Modern Optics*, 56(6):722–728, 2009.
- [61] Wayne Lawton, Anders S Mouritzen, Jiao Wang, and Jiangbin Gong. Spectral relationships between kicked harper and on-resonance double kicked rotor operators. *Journal of mathematical physics*, 50(3):032103, 2009.
- [62] Hailong Wang, Derek YH Ho, Wayne Lawton, Jiao Wang, and Jiangbin Gong. Kicked-harper model versus on-resonance double-kicked rotor model: From spectral difference to topological equivalence. *Physical Review E*, 88(5):052920, 2013.
- [63] Mahmoud Lababidi, Indubala I Satija, and Erhai Zhao. Counter-propagating edge modes and topological phases of a kicked quantum hall system. *Physical review letters*, 112(2):026805, 2014.
- [64] Zhenyu Zhou, Indubala I Satija, and Erhai Zhao. Floquet edge states in a harmonically driven integer quantum hall system. *Physical Review B*, 90(20):205108, 2014.
- [65] Kai-He Ding, Lih-King Lim, Gang Su, and Zheng-Yu Weng. Quantum hall effect in ac driven graphene: From the half-integer to the integer case. *Physical Review B*, 97(3):035123, 2018.
- [66] Martin Wackerl, Paul Wenk, and John Schliemann. Driven hofstadter butterflies and related topological invariants. *Physical Review B*, 100(16):165411, 2019.
- [67] SH Kooi, A Quelle, W Beugeling, and C Morais Smith. Genesis of the floquet hofstadter butterfly. *Physical Review B*, 98(11):115124, 2018.
- [68] Ming Zhao, Qi Chen, and Liang Du. Floquet engineering the hofstadter butterfly in the square lattice and its effective hamiltonian. *Journal of Physics A: Mathematical and Theoretical*, 55:275003, 2022.
- [69] Nadia Benlakhrou, Ahmed Jellal, Hocine Bahlouli, and Michael Vogl. Chiral limits and effect of light on the hofstadter butterfly in twisted bilayer graphene. *Physical Review B*, 105(12):125423, 2022.
- [70] Michael Vogl, Martin Rodriguez-Vega, and Gregory A Fiete. Effective floquet hamiltonians for periodically driven twisted bilayer graphene. *Physical Review B*, 101(23):235411, 2020.
- [71] Grigory Tarnopolsky, Alex Jura Kruchkov, and Ashvin Vishwanath. Origin of magic angles in twisted bilayer graphene. *Physical review letters*, 122(10):106405, 2019.
- [72] Yantao Li, HA Fertig, and Babak Seradjeh. Floquet-

engineered topological flat bands in irradiated twisted bilayer graphene. *Physical Review Research*, 2(4):043275, 2020.

- [73] Or Katz, Gil Refael, and Netanel H Lindner. Optically induced flat bands in twisted bilayer graphene. *Physical Review B*, 102(15):155123, 2020.
- [74] Francisco Guinea and Niels R Walet. Continuum models for twisted bilayer graphene: Effect of lattice deformation and hopping parameters. *Physical Review B*, 99(20):205134, 2019.
- [75] Liang Du, Qi Chen, Aaron D Barr, Ariel R Barr, and Gregory A Fiete. Floquet hofstadter butterfly on the kagome and triangular lattices. *Physical Review B*, 98(24):245145, 2018.
- [76] Stephen Carr, Shiang Fang, Ziyang Zhu, and Efthimios Kaxiras. Exact continuum model for low-energy electronic states of twisted bilayer graphene. *Physical Review Research*, 1(1):013001, 2019.
- [77] Hossein Dehghani, Takashi Oka, and Aditi Mitra. Out-of-equilibrium electrons and the hall conductance of a floquet topological insulator. *Physical Review B*, 91(15):155422, 2015.
- [78] Martin Rodriguez-Vega, Michael Vogl, and Gregory A Fiete. Low-frequency and moiré-floquet engineering: a review. *Annals of Physics*, 435:168434, 2021.
- [79] John David Jackson. Classical electrodynamics, 1999.

Appendix A: CALCULATION OF HOFSTADTER BUTTERFLY

In the presence of a perpendicular magnetic field, $\mathbf{B} = B\hat{z}$, we substitute $\hat{\mathbf{p}} \rightarrow \hat{\mathbf{p}} + e\mathbf{A}$. We use the Landau gauge $\mathbf{A} = B(-y, 0)$ and rewrite the intralayer Hamiltonian as

$$h(\theta/2) = \omega_c \left[\frac{\sigma_x + i\sigma_y}{2} e^{i\theta/2} a + \frac{\sigma_x - i\sigma_y}{2} e^{-i\theta/2} a^\dagger \right] \quad (\text{A1})$$

where $\omega_c = \sqrt{2}v_F/\ell_b$ is the cyclotron energy, $\ell_b = \sqrt{1/eB}$ is the magnetic length, and

$$a^\dagger = \frac{\ell_b}{\sqrt{2}} [p_x - eBy + ip_y], \quad (\text{A2})$$

$$a = \frac{\ell_b}{\sqrt{2}} [p_x - eBy - ip_y] \quad (\text{A3})$$

are the raising and lowering operators of LL index. It is straightforward to demonstrate that $[a, a^\dagger] = 1$, and they act on the Landau-level n -th eigenstate as follows

$$a |n\rangle = \sqrt{n} |n-1\rangle, \quad (\text{A4})$$

$$a^\dagger |n\rangle = \sqrt{n+1} |n+1\rangle. \quad (\text{A5})$$

The Hamiltonian can be diagonalized numerically using the LLs basis $|L, n, \alpha, y_c\rangle$ where $L = 1, 2, 3$ represents the layers, $\alpha = A, B$ represents sublattices, n represents LL index, and y_c is the guiding center. The guiding centers in $T_{2,3}$ interlayer hopping terms shift y_c by $\pm\Delta$. Thus, one can write

$$y_c = y_0 + (mq + j)\Delta, \quad (\text{A6})$$

with $j \in \{0, 1, \dots, q-1\}$, and $\Delta = \sqrt{3}k_\theta\ell^2/2$. The moiré unit-cell must be commensurate with the magnetic unit-cell such that the associated Hamiltonian becomes diagonalizable for

a system of infinite size. The magnetic flux ϕ through the unit-cell is given by [5]

$$\phi = \frac{q}{p}\phi_0, \quad \phi_0 = \frac{hc}{e}, \quad (\text{A7})$$

where $p/q \in \mathbb{Q}$ the rational number connecting the size of bare magnetic and moiré Brillouin zones when both lattices are commensurate. To be more specific, the end result of the magnetic moiré Brillouin zone (MMBZ) is limited by

$$0 < k_x = \frac{y_0}{\ell^2} < \frac{4\pi p}{qk_\theta\ell^2}, \quad 0 < k_y < \frac{4\pi}{\sqrt{3}k_\theta q}. \quad (\text{A8})$$

The Fourier transform thus offers a computationally convenient basis

$$|L, n, \alpha, j\rangle = \frac{1}{\sqrt{N}} \sum_m e^{ik_y(mq+j)\Delta} |L, n, y_0 + (mq + j)\Delta\rangle. \quad (\text{A9})$$

We are forced to remove k_y from the basis because the Hamiltonian is diagonal in k_y . The intralayer Hamiltonian in terms of the basis in Eq. A9 is written as

$$h(\theta/2) = \omega_c \sum_{L,n,j} \left(e^{-i\theta/2} \sqrt{n+1} |L, n+1, A, j\rangle \langle L, n, B, j| \right) + \text{H.c.} \quad (\text{A10})$$

The interlayer Hamiltonians, on the same basis, are

$$\begin{aligned} T_{12}(\mathbf{k}) = & \sum_{n'\alpha\beta j} \left[T_1 F_{n'n}(\mathbf{z}_1) e^{-ik_x k_\theta \ell^2} e^{-4\pi i \frac{p}{q} j} |2n'\alpha j\rangle \langle 1n\beta j| \right. \\ & + T_2 F_{n'n}(\mathbf{z}_2) e^{ik_y \Delta} e^{\frac{i}{2} k_x k_\theta \ell^2} e^{i\pi \frac{p}{q} (2j-1)} |2n'\alpha, j+1\rangle \langle 1n\beta j| \\ & \left. + T_3 F_{n'n'}(\mathbf{z}_3) e^{-ik_y \Delta} e^{\frac{i}{2} k_x k_\theta \ell^2} e^{i\pi \frac{p}{q} (2j+1)} |2n'\alpha j-1\rangle \langle 1n\beta j| \right], \end{aligned} \quad (\text{A11})$$

$$\begin{aligned} T_{23}(\mathbf{k}) = & \sum_{n'\alpha\beta j} \left[T_1 |3n'\alpha j\rangle \langle 2n\beta j| + T_2 |3n'\alpha, j+1\rangle \langle 2n\beta j| \right. \\ & \left. + T_3 |3n'\alpha j-1\rangle \langle 2n\beta j| \right], \end{aligned} \quad (\text{A12})$$

with $\mathbf{z}_j = \frac{qj_x + iqj_y}{\sqrt{2}} \ell_b$, and

$$F_{nm}(\mathbf{z}) = \begin{cases} \tilde{F}_{nm}(\mathbf{z}) & n \geq m \\ \tilde{F}_{nm}^*(-\mathbf{z}) & m < n \end{cases} \quad (\text{A13})$$

$$\tilde{F}_{nm}(\mathbf{z}) = \sqrt{\frac{m!}{n!}} e^{-\frac{\mathbf{z}^2}{2}} (-z_1 + iz_2)^{n-m} \mathcal{L}_m^{n-m}(\mathbf{z}^2)$$

where \mathcal{L} is referred to as the associated Laguerre polynomial. It is crucial to clarify one subtlety concerning this Hamiltonian's numerical implementation, which was emphasized as a footnote in [5]. While the Hamiltonian is simple to execute numerically for the most part, one must be cautious when including states to prevent a false degeneracy at low energies. Consider the case where we are unaware of the interlayer couplings because we chose a model that is relevant near the graphene K point. We must realize that there is only one eigenstate with K point and zero energy per layer. On the other hand, if we choose our fundamental states from

$$\{L \in \{t, m, b\}, \alpha \in \{A, B\}, n \in \{0, \dots, n_{\max}\}\}, \quad (\text{A14})$$

and then diagonalize at zero energy, we identify more wrong states. At the K point, we could now relate back to the

wavefunctions and analytical equations of the zero energy LL for graphene. At each layer we have $|n, \pm\rangle = (\pm|n-1\rangle, |n\rangle)$. The only contributions from sublattice B appear to be $n=0$ in this case. Since our basis choice does not violate sublattice symmetry, we can assume that the existence of zero energy states with contributions from sublattice A is a numerical artifact. The solutions certainly violate sublattice symmetry, and we must guarantee that this strengthens our numerical method. To do this, a slightly different set of basis states that violate sublattice symmetry is used. Below, we mention such

a possibility

$$\{L \in \{t, m, b\}, \alpha \in \{A, B\}, n \in \{0, \dots, n_{\max} - \delta_{\alpha, B}\}\}. \quad (A15)$$

False states are pushed to higher energies as a result of the explicit breakdown of sublattice symmetry in this choice of basis states, but this has no relevance to our situation [5]. While we emphasize this, when it comes to non-coupling layers, the false low lying levels do not appear. This point is less important in a plot of LLs (because the content does not show degeneracy), but it becomes very helpful in the case of interlayer coupling. Interestingly, LLs are split as interlayer couplings are added, and false low energy bands have a disastrous impact. As a result, it is critical to eliminate the erroneous contributions using the method we just outlined [69].